Design Optimization of a Solid Rocket Motor for a Suborbital Space Flight

Y. Kamm, D. Horowitz*, N. Brauner** and A. Gany****

**Israel Military Industries Ltd. (IMI), P.O. Box 1044, Ramat Hasharon 47100, Israel*

***Tel-Aviv University, School of Mechanical Engineering, Tel-Aviv 69978, Israel*

**** Technion – Israel Institute of Technology, Faculty of Aerospace Engineering, Haifa 32000, Israel*

Abstract

This work uses an advanced algorithm and representative subsystem physical models to optimize the design of a solid rocket motor. A single stage vertical launch of a 1500 kg capsule to an altitude of 100 km with an acceleration limit of 3g is considered. The various motor subsystems are modelled and integrated with the ballistic equations. A genetic algorithm optimizes the design for the required mission. The parameters examined are motor pressure, expansion ratio, burn time, thrust profile, nozzle exit angle and length-to-diameter ratio. A sensitivity study of the different parameters is also performed.

Nomenclature

A	motor cross section area
a	acceleration
c	constant
c^*	characteristic velocity
C_D	drag coefficient
C_F	thrust coefficient
C_f	fiber slip coefficient in winded casing
D	casing outer diameter
D.P.	dynamic pressure
er	erosion
F	thrust
g_0	gravity acceleration at sea level
h	altitude
k_p	initial to average pressure ratio
L	length
m_0	initial mass
m	mass
p	motor pressure
p_c	average motor pressure
R	cylinder radius
R_0	Earth radius
R_e	nozzle exit radius
R_s	upstream throat radius
R_t	throat radius
r	radius
r_c	casing covering opening radius
r_0	winded casing opening radius
t	time
t_b	motor burn time
V	volume
v	velocity
w	thickness
WF	web fraction
w_{Th}	insulation throat thickness
z	motor axis

Greek

ε	expansion ratio
η	efficiency
θ_e	nozzle exit angle
θ_i	nozzle inflection angle
ρ	density
σ	maximum strain

subscripts

a	atmospheric
comp	composite fiber
f, fwd	forward
gd	grain design
ins	insulation
J	nozzle flexible joint
L	payload
noz	nozzle
p	propellant
r	rear
s	inert structure
str	metal structure
sub	submerged

Unless otherwise stated, all units are MKS, pressure in atmospheres

1. Introduction

In the preliminary design stage of a solid rocket motor, there are many design parameters whose values are difficult to determine initially (e.g., chamber pressure, expansion ratio, etc.), necessitating the design modeling and optimization for the specific mission. In the design of a rocket motor, the performance of the system should be maximized, as defined by an objective function, e.g., the "total-weight-to-payload" ratio, which is often used[1,2,3] as a measure of the system's efficiency, and is also used in this work. Other criteria used in other works are added velocity[1,4], maximum range[5,6] and cost[1,2,3,4]. The usual constraints are maximum acceleration, dynamic pressure and geometric dimensions. The optimization methods used in the past include simple gradient searches and more recently, genetic algorithms. In this work, the emphasis is placed on the detailed description of the structural models used and the subsystem dependencies, which are lacking in other works.

This paper describes in detail the design optimization of a single stage solid rocket motor. The mission was defined to be the launch of 1500 kg capsule to an altitude of 100 km with a dynamic pressure limit of 1 atmosphere and an acceleration limit of 3g. This relatively simple mission is used to illustrate the principles of the optimization method of the various design parameters. A genetic algorithm optimization was performed on six design parameters: motor pressure, expansion ratio, nozzle exit angle, pressure profile, length to diameter ratio and burn time.

2. Solution principles

The external conditions and trajectory losses are important and affect the design and therefore must be included in the optimization process even though this causes an increase in the computation time. The general optimization process is described in Figure 1. Since the mission characteristics (e.g., drag and gravity losses, maximum dynamic pressure, maximum acceleration, required propellant mass, etc.) are not known in advance, an iterative process must be established to ensure the mission (in this case – a maximum altitude of 100 km) is achieved under the given trajectory constraints (maximum dynamic pressure of 1 atmosphere and maximum acceleration of 3g) and inherent structural constraints. In this process, the design parameters (motor pressure, expansion ratio, motor burn time, thrust profile, etc.) are changed until an optimum is found. In other words, the program "designs" the motor (based on the design parameters) and calculates the trajectory. If any structural or trajectory constraints are broken, the design parameters are changed and a new motor is designed. If the required maximum altitude is not achieved, the propellant weight is adjusted accordingly and a new motor is designed; otherwise, the objective function (m_0/m_L) is returned to the optimization program for a new set of design parameters until ultimately, an optimum design is achieved.

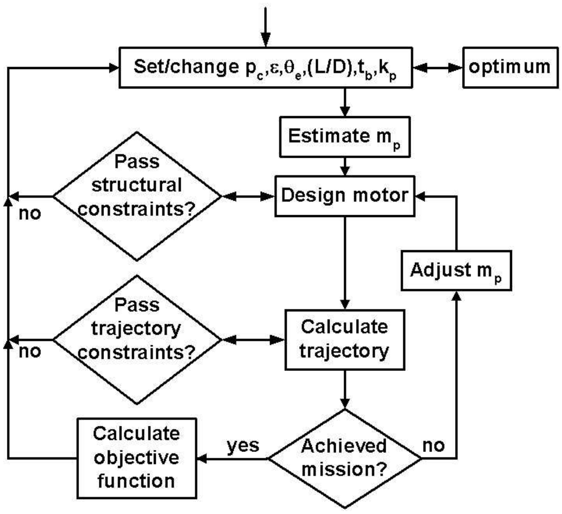

Figure 1: Overall solution logic

There are many complex dependencies among the various design parameters of the motor that necessitate an iterative process to converge to the desired work point. The important parameters (mass, length, etc) of the various subsystems are calculated by approximate physical and empirical models in order to facilitate the optimization. Another important aspect in the design optimization is the grain design and thrust profile. It would be highly desirable to include the grain design (via the thrust profile) in the optimization process. However, this would entail excessive computation time, especially since different grain designs often result in similar thrust profiles. Including the grain design in the optimization process would necessitate a very efficient, three-dimensional geometric code even if it were not coupled to the internal flow equations. For these reasons, it was decided, at this stage, to assume a simple linear (neutral, progressive or regressive) thrust profile generated by a single parameter k_p (initial to average thrust ratio) that is included in the optimization process. Obviously, the grain design, volumetric loading ratio, surface exposure areas all depend on k_p and should also be part of the optimization process. In this work this dependence is only partially modeled, but an improved model is being developed and will be presented in a future paper.

3. Motor structure

As shown schematically in Figure 2, the motor consists of three main systems (propellant, winded casing and nozzle) along with the appropriate subsystems (insulation, flexible joint, covers, etc.). The main challenge in this work was to simplify and model the complex relations between the different subsystems. Usually, these subsystems are designed after a lengthy numerical analysis using complicated computer programs. These computer codes are not suitable for the level of modeling needed for an efficient optimization process. Therefore it was necessary to simplify the models and develop an analysis that would be simple and efficient enough to run repeatedly in the optimization calculations yet accurate enough for the preliminary design.

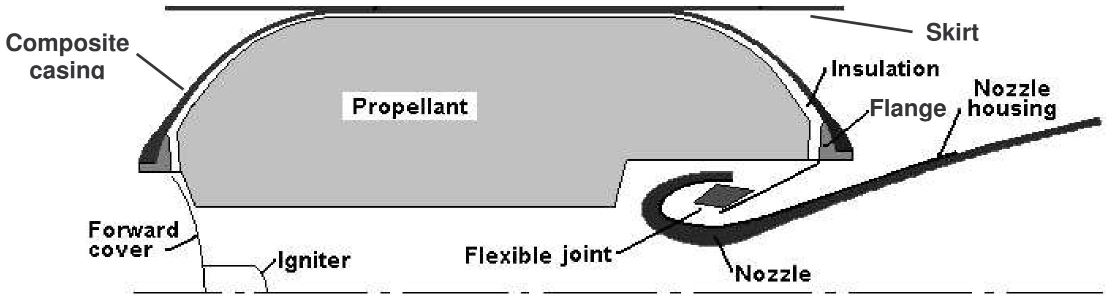

Figure 2: Schematic drawing of the solid propellant motor subsystems

4. Design and analysis of the motor

As described in Figure 1, the trajectory is calculated every time a motor is "designed" based on a new set of design parameters and the required propellant mass m_p. The program calculates the dimensions and weights of the various subsystems. The main design variables are shown in Figure 3.

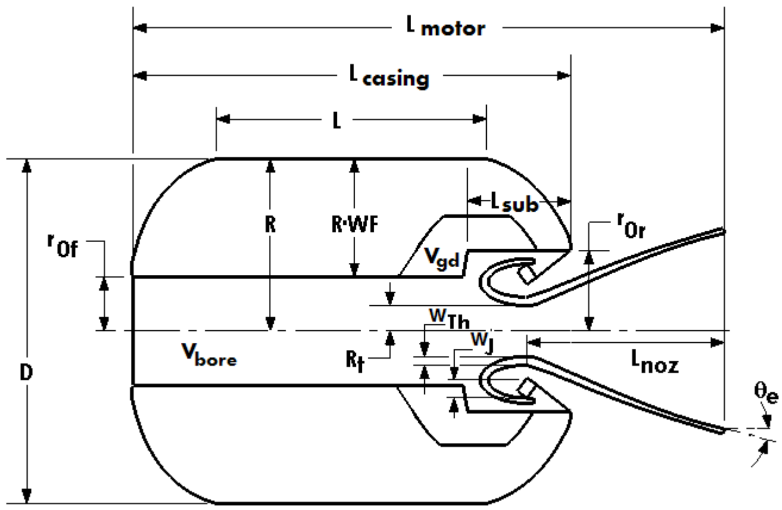

Figure 3: Geometric design variables

The design flow is shown in Figure 4, where the propellant mass and the six known design parameters are in circles and the design variables to be calculated (based on the design parameters) are in squares. The calculation sequence starts with the propellant mass that is known for the current work point. The thin lines show the interconnectivity between the known design parameters and the calculated design variables. The equations and constraints are outlined in the Appendix and are briefly reviewed here:

- The throat radius R_t is calculated as a function of m_p, p_c and t_b (Eq. 6).
- The insulation thickness at the throat (w_{Th}) is calculated as a of function p_c, t_b, R_t (Eq. 13).
- The thickness of the flexible joint w_J is a function of only R_t and w_{Th} (the pressure dependence is neglected).
- The rear casing opening radius r_{0r} is calculated and depends on the calculated variables R_t, w_{Th} and w_J (Eq. 11)
- The propellant web fraction WF is taken to be the maximum possible from a strain standpoint and therefore is a function of L/D, p_{max} and propellant properties (Eq. 21). In addition, to ensure that no erosive burning exists, the port radius must be at least 40% greater than the throat radius (Eq. 22).
- The radius of the casing R is obtained by an iterative calculation until the desired propellant mass is obtained:
    - A value for R is assumed and the forward casing opening radius r_{of} is calculated (as a function of R, L/D, r_{or} and C_f), (Eq. 23).
    - The volume of the empty casing V_{casing} is calculated, depending on R, r_{or}, L/D and r_{of} (Eq. 8).
    - The bore volume (the volume without propellant) is a function of L_{sub}, WF and L_{casing} (Eq. 9).
    - The insulation volume is calculated as a function of p_c, t_b, L/D, and k_p (Eq. 16).
    - The propellant mass is calculated by subtracting the port, insulation and other volumes from the casing volume (Eq. 10).
    - This calculated mass is compared with the required mass, and if they do not match, the casing radius R is adjusted accordingly and the calculation repeated until the masses converge.

The subsystem masses are then calculated: nozzle (Eqs. 14,19,20), winding (Eq. 15), casing insulation (Eq. 16), flanges (Eq. 17) and forward cover (Eq. 18).

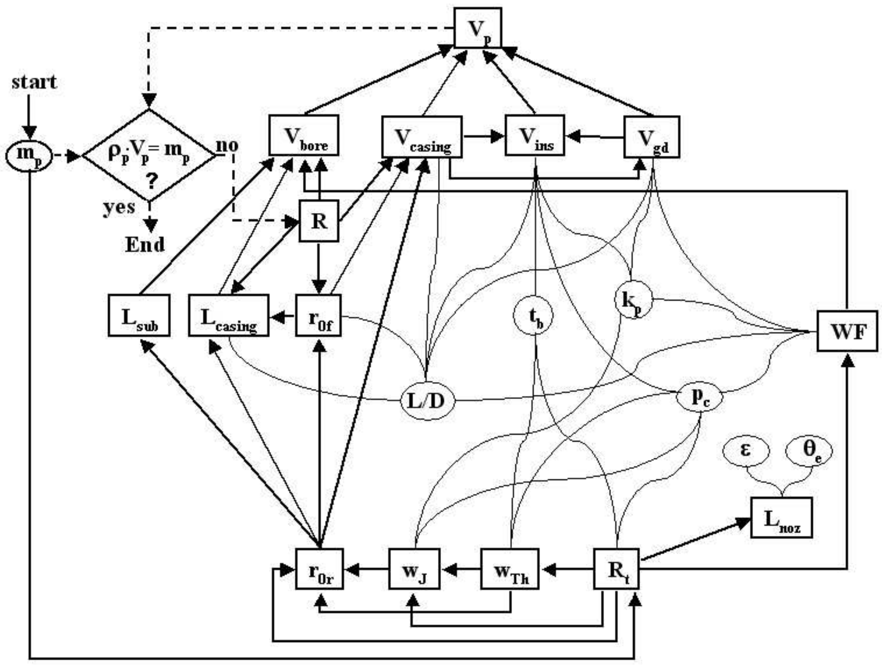

Figure 4: Geometric design variable and parameter interdependencies

4.1 Design of the nozzle insulation

The nozzle insulation is one of the more complicated subsystems in the rocket motor. The analysis and design is usually done by the use of complex heat transfer programs but for the optimization code, a simpler approach was used. As shown in Figure 5, the forward part of the nozzle insulation (sections AA, BB and CC) is defined by four elliptic profiles (two internal and two external), while the profile downstream of the throat is described by a 2^{nd} degree polynomial. This enables the geometric control of the insulation thickness needed at the different sections, while allowing for the necessary gap for the flexible joint, even at different insulation thicknesses, as shown by the different nozzles in Figure 5.

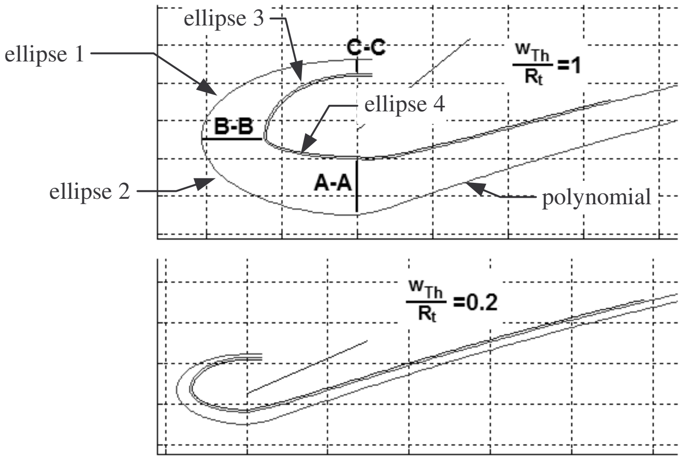

Figure 5: Comparison of nozzle insulation thickness for two different nozzles

Figure 6 compares the insulation thickness of this work (polynomial and ellipses) with the actual insulation of the Titan IV nozzle[7].

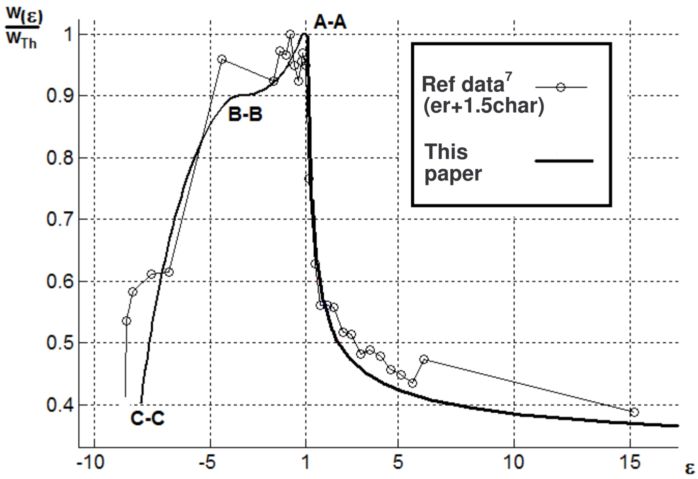

Figure 6: Comparison of designed and actual nozzle insulation for the Titan IV nozzle

In order to simplify the optimization process, it is proposed that the insulation calculation along the nozzle can be divided into the geometry effects (throat radius, expansion ratio and exit angle), motor conditions (burn time and pressure) and insulation characteristics, Eq. 13 and 14.

4.2 Design of the winded casing

The casing is the heaviest inert component of the motor and also directly affects the available propellant volume. Approximate analytical models were developed for the calculation of the composite casing mass (which depends on r_0/R and L/D) and internal dome profile, Eqs. 15 and 8 respectively.

4.3 Design of the casing insulation

After the winded casing, the insulation is the second heaviest inert component, and is influenced by the exposure times along the casing (which are a result of the grain design which is affected by L/D) and motor pressure. Equation 16 separates the motor conditions (p_c and t_b) from the geometric aspects in the calculation of the insulation mass.

5. Optimization results and discussion

The optimization objective function was set as the initial weight to payload mass ratio (m_0/m_L), but other objectives can easily be defined. The following ranges were set for the six design parameters: t_b=40-60 sec, L/D=1-5, p_c=50-100 atm, k_p=0.5-1.5, ε=9-30, θ_e=3-15 deg. Preliminary computer runs were made to establish the stability and the system behavior. In a random (simple search) run of 5000 design sets, only 2% yielded motors that were viable (i.e., passed the structural criteria). The consequence is increased computer run times since most runs are "wasted" on useless motors. It was observed that the constraints caused many local minimum solutions making a gradient search ineffective.

When a genetic algorithm was used, after 100 generations (Figure 7) with 1160 sample points (68% of them were within the constraint limits), a minimum of 2.30 was achieved for m_0/m_L. A local gradient search around this minimum yielded an improved result of 2.289 for m_0/m_L, with the following design parameters: t_b=48.33 sec, L/D=4.41, p_c=72.16 atm, k_p=1.290, ε=13.95, θ_e=6.17 deg. Other design values at the optimum include: m_p=1790 kg, m_s=143.6 kg, WF=0.728, burn rate (at 70 atm)=5 mm/s, R_t=0.0491 m, R=0.329, r_{0r}/R=0.623. Each sample point took approximately 2.3 seconds CPU time. Compared to a simple search, the genetic algorithm was found to be more suitable. The motor at the optimized design point is presented in Figure 8.

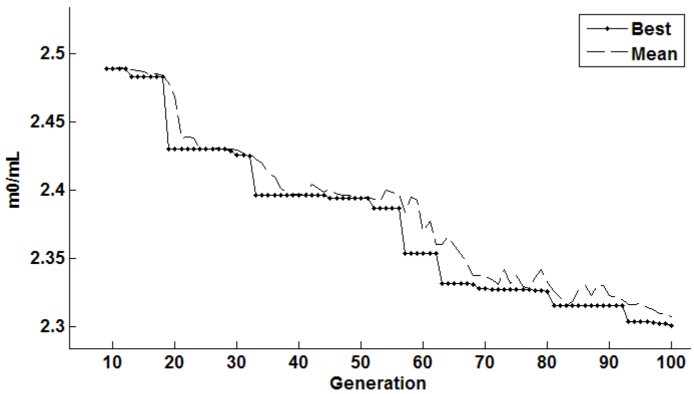

Figure 7: Optimization results

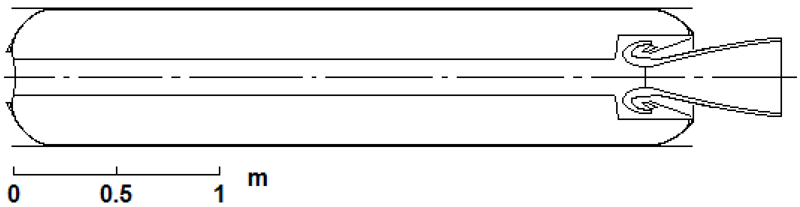

Figure 8: Motor configuration at optimum

The missile trajectory and performance during the motor burn time (normalized to the parameters' maximum values) are shown in Figure 9, with the following maximum values: v_{max}=1186 m/s, h_{max}(at burnout)=26,922 m, F_{max}=110 kN, m_0=3,434 kg, D.P.$_{max}$=1.00 atm, a_{max}=3.00 g, p_{max}=93 atm, C_{Dmax}=0.41 . The maximum required height of 100 km occurs after approximately 180 seconds. In Table 1 the mass distribution of the motor is presented:

Table 1: Mass distribution of the motor subsystems

Motor subsystem	Mass (%)
Propellant	92.57
Winded casing	2.74
Internal casing insulation	1.46
Nozzle insulation	0.74
Nozzle metal structure	0.32
Flexible joint	0.12
Flanges	0.10
Forward cover	0.09
Other	1.86

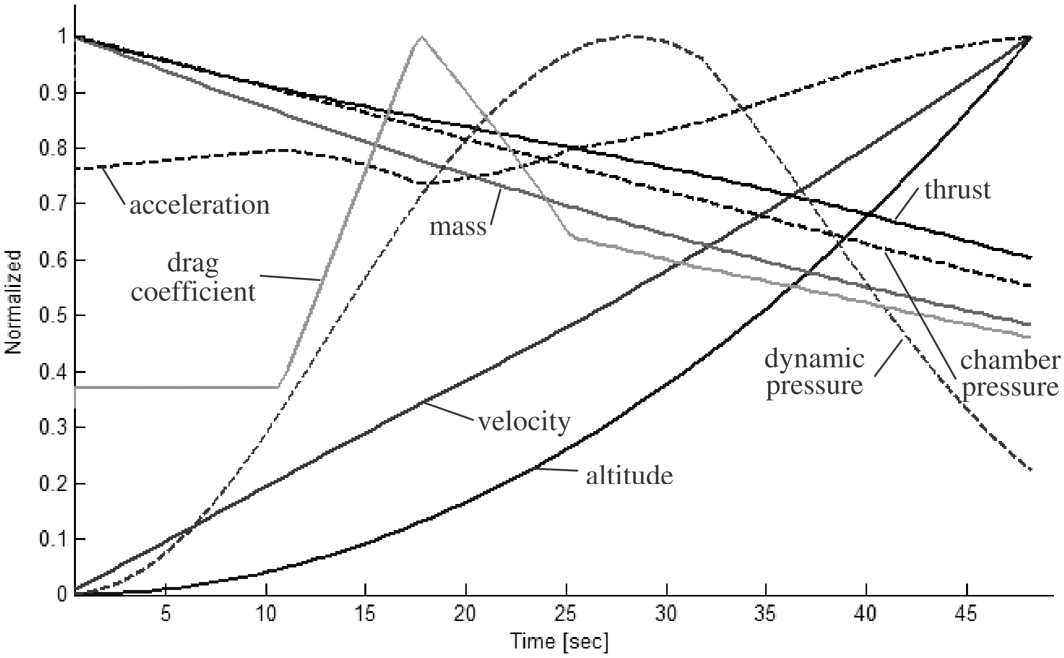

Figure 9: Trajectory and mission parameters during motor burn

The following observations can be made upon examination of the results of the various computer runs:

- The thrust slope is larger than the pressure slope because of the decreasing atmospheric pressure (and increasing thrust coefficient).
- The acceleration slightly decreases when the missile passes through Mach 1 because of the increased drag.
- If the limit on the dynamic pressure is removed, the optimized value of k_p increases from 1.290 to 1.375.

5.1 Parameter sensitivity check

In order to understand the influence of the parameters on the design, each design parameter was independently changed up to ±10% (in steps of 1%) around the optimum point and the objective function (m_0/m_L) was calculated, regardless of the various constraints. The results are shown in Figure 10.

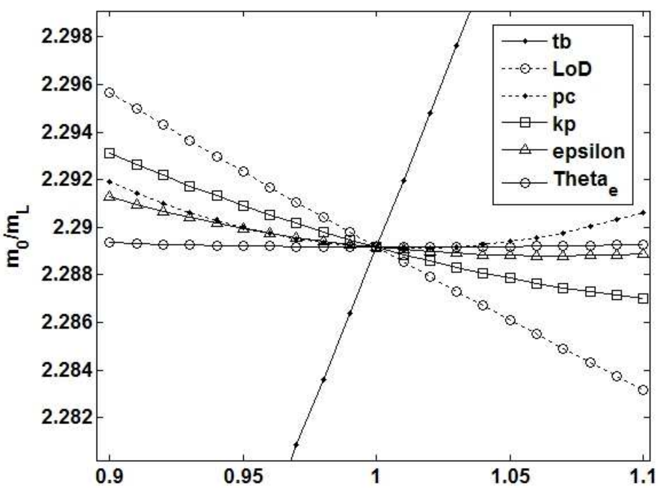

Figure 10: Objective sensitivity to design parameters

As can be seen in Fig. 10, the order of the effect of the design parameters on the objective function is: t_b, L/D, k_p, p_c, ε, θ_e. From an analysis of the results, some of these design parameters are limited by the constraints:

- The burn time is limited by the acceleration constraint (a short burn time lowers the gravitational losses).

- The length to diameter ratio (L/D) is determined by the lower burn rate limit. A larger L/D leads to lower drag losses (when the burn rate constraints are removed, the optimum is shifted to a larger L/D).
- The initial to average pressure ratio (k_p) is limited by the maximum dynamic pressure. A higher k_p straightens the acceleration profile and (up to a point) lowers the gravitational losses (more than the increased drag losses).

The other design parameters arrive at their optimum through a trade-off between performance and mass considerations:

- A higher average motor pressure (p_c) means a higher specific impulse, which means an improved motor performance needing less propellant. Of course, a higher pressure means a heavier casing so at some point raising the pressure does not improve motor performance..
- The expansion ratio of the nozzle (ε) should, in general, be adapted to the external pressure of the trajectory during the motor burn, but a larger ε also means a heavier nozzle.
- A larger nozzle exit angle (θ_e) means a shorter (and lighter) nozzle even though the divergence losses will be slighter higher.

5.2 Optimization method efficiency

The use of a genetic algorithm increased the number of viable sample points from 5% to 50% as compared to a random or simple search. With only six parameters in the present design set, this increased efficiency was not especially noticeable. But if the mission involves a three-stage missile, the number of parameters jumps to at least 20, and the use of a genetic algorithm is definitely warranted.

6. Conclusions

An optimization method for the design of a solid rocket is presented in detail along with the parameters and models used. If and when more exact models become available for the various motor subsystems, they can easily be incorporated into the code, because of the modular structure of the software. The relations between the various design variables are shown and an optimum found for a single-stage suborbital mission. The principles and methods presented can be used for multi-staged rockets and more complicated missions.

References

1. Chiang, M.J., Y.P. Su., S.D. Chang. The Optimization of Solid Rocket Vehicles. *AIAA/SAE/ASME 19th Joint Propulsion Conference*, Seattle, WA, June 27-29, AIAA-83-1251, 1983.
2. Calabro, M., A. Dufour and A. Macaire. Optimization of the Propulsion for Multistage Solid Rocket Motor Launchers. *J. Acta Astronautica*, 50: 201-208, 2002.
3. Shelton, J., R.A. Frederick and A.W. Wilhite. Launch Vehicle Propulsion Design with Multiple Selection Criteria. *AIAA/SAE/ASME 41st Joint Propulsion Conference*, Tucson, Arizona, July 10-13, AIAA 2005-3851, 2005.
4. Trulove, A.M. and K.W. Whitaker. Rocket Stage Optimization Using a Simple Genetic Algorithm. *AIAA/SAE/ASME 29th Joint Propulsion Conference,* Monterey, CA, July 10-13, AIAA-93-1778, 1993
5. Jacques, L. and J. Roux. Computer Aided Preliminary Design of Solid Rocket. *AIAA/SAE/ASME 19th Joint Propulsion Conference*, Seattle, WA, June 27-29, AIAA-83-1251, 1983.
6. Anderson, M.B., J.E. Burkhalter and R.M. Jenkins. Multi-Disciplinary Intelligent Systems Approach to Solid Rocket Motor Design. *AIAA/SAE/ASME 37th Joint Propulsion Conference*, Salt Lake City, UT, June 8-11, Part I & II AIAA-2001-3599 & AIAA 2001-3600, 2001.
7. Johnstun, W. Performance of Different Ablator Materials on the Titan IV SRMU Nozzles. *AIAA/SAE/ASME 37th Joint Propulsion Conference*, Salt Lake City, UT, June 8-11, AIAA 2001-3437, 2001.
8. Sutton, G.P. and O. Biblarz. Rocket Propulsion Elements. 7th Ed., John Witey & Sons Inc., N.Y., 2001.
9. Vasiliev, V.V., A.A. Krikanov and A.F. Razin. New generation of filament-wound composite pressure vessels for commercial applications. *J. Composite Structures*, 62: 449-459, 2003.
10. Hill, P.G. and C.R. Peterson. Mechanics and Thermodynamics of Propulsion. 2nd Ed., pp. 550-551. Addison-Wesley Co., N.Y., 1992.
11. Peters, S.T., W.D. Humphrey and R.F. Foral. Filament Winding Composite Structure Fabrication. 2nd Ed., SAMPE Int., Covina, CA., 1999.
12. Solid Rocket Motor Internal Insulation. *NASA SPACE VEHICLE DESIGN CRITERIA (CHEMICAL PROPULSION),* NASA Monograph SP-8093, December 1976.
13. Solid Propellant Grain Structural Integrity Analysis. *NASA SPACE VEHICLE DESIGN CRITERIA (CHEMICAL PROPULSION),* NASA Monograph SP-8073, June 1971.

Appendix – Main equations, formulas and constraints

As mentioned before, in order to shorten calculation times, it is necessary to develop simple models to describe complex systems whose design depends on many variables. If possible, these models should not need iterative, time-consuming converging solutions, but rather supply a quick estimate of the required parameter. For this reason, many of the equations are approximations in polynomial or power forms and are derived from regression analysis of results obtained from finite-element design techniques. Many of the equations contain constants that depend on materials and the personal preferences of the designer.

External ballistics[8] for vertical launch:

$$\frac{dv}{dt} = \frac{F}{m} - \left(\frac{0.5\rho_{Air} A C_D}{m}\right) v^2 - g_0 \left(\frac{R_0}{R_0 + h}\right)^2 \quad \textbf{(1)}$$

$$\frac{dh}{dt} = v \quad \textbf{(2)}$$

Internal ballistics[8]:

$$p_{(t)} = p_c \left[k_p - 2(t/t_b)(k_p - 1)\right] \quad \textbf{(3)}$$

$$F_{(t)} = \eta_{(\theta_e)} C_{F(\varepsilon, p, p_a, \gamma)} p_{(t)} \pi R_t^2 \quad \textbf{(4)}$$

$$\eta_{(\theta_e)} = 0.94\left(1 + \cos\theta_e\right)/2 \quad \textbf{(5)}$$

$$R_t = \left(\frac{c^* m_p}{\pi t_b p_c}\right)^{0.5} \quad \textbf{(6)}$$

Composite casing dome profile[9]:

$$\frac{d^2 z}{dr^2} = \frac{dz}{dr}\left[1 + \left(\frac{dz}{dr}\right)^2\right]\left(\frac{2r}{r^2 - r_c^2} - \frac{r_0^2}{r^3 - r_0^2 r}\right) \quad \textbf{(7)}$$

Inner lengths and volumes:

Integrating Eq. 7 under the right conditions[9] yields the approximate volume and length of the domes and casing (assuming $r_c^2 << R^2$):

$$\begin{aligned} \frac{V_{dome}}{R^3} &= 0.85\left(\frac{r_0}{R}\right) + 1.4 \\ \frac{L_{dome}}{R} &= 0.154\left(\frac{r_0}{R}\right) + 0.5225 \end{aligned} \Rightarrow \begin{aligned} \frac{V_{casing}}{R^3} &= 2\pi\left(\frac{L}{D}\right) + 0.85\left(\frac{r_{0r} + r_{0f}}{R}\right) + 2.8 \\ \frac{L_{casing}}{R} &= \frac{L}{R} + 0.154\left(\frac{r_{0r} + r_{0f}}{R}\right) + 1.045 \end{aligned} \quad \textbf{(8)}$$

The minimum volume of the inner bore, including space for the submerged nozzle:

$$\frac{V_{bore}}{R^3} = \pi\left[\left(1 - WF\right)^2\left(\frac{L_{casing} - L_{sub}}{R}\right) + \frac{r_{0r}^2 L_{sub}}{R^3}\right] \quad \textbf{(9)}$$

The actual value of the web fraction WF is determined by the propellant's strain properties. The nozzle submergence length L_{sub} is assumed to be $1.5r_{0r}$. In addition to V_{bore}, an additional "grain design" volume (V_{gd}), such as radial slots etc., is assumed which is a function of k_p, L/D and throat erosion. The remaining volume available for the propellant is calculated by subtracting all other volumes (insulation, inner bore, grain design) from the casing volume:

$$V_p = V_{casing} - V_{ins} - V_{bore} - V_{gd} \tag{10}$$

Substituting the approximations of Equations 8 and 9 and the constraints of equations 21 and 23 into equation 10 allows the design for a set of design parameters under the structural constraints.

Rear casing opening and nozzle assembly:

The rear casing opening depends on the throat radius R_t, nozzle insulation thickness, flexible joint width and the appropriate spacing ($0.5w_{Th}+0.6R_t$), as shown in Figure 3. The flexible joint width w_J is assumed for simplicity to depend on the throat radius and the throat insulation thickness (and not on the motor pressure): $w_J=(w_{Th}+R_t)/2$. The insulation thickness above the flexible joint (section C-C in Figure 5) is assumed to be $0.4w_{Th}$. The dependence of the rear casing opening on the throat radius is therefore:

$$\frac{r_{0r}}{R_t} = 2.4\frac{w_{Th}}{R_t} + 2.1 \tag{11}$$

The aft (downstream) profile of the nozzle is described by a 2nd degree polynomial:

$$r_{(z)} = R_t + R_s\left(1-\cos\theta_i\right) + \tan\theta_i X + \left(\frac{\tan^2\theta_e - \tan^2\theta_i}{4\left(R_e - R_t - R_s\left(1-\cos\theta_i\right)\right)}\right)X^2 \tag{12}$$

where X= $z - R_s \sin\theta_i$ (to move the origin). The above profile starts where the curvature radius of the throat (R_s) is tangent to the initial angle of the contoured nozzle θ_i.

The nozzle insulation thickness (w_{Th}) is set to be the erosion depth + 1.5 the char depth ($w_{Th}=er+1.5char$), where the erosion[10] and char are calculated, Eq. 13. The model for the char depth was assumed to be in a similar form as the erosion depth model, after comparison with experimental results.

$$\begin{aligned} er &= \left(e_r\right)_{ref}\left[\frac{p_c}{\left(p_c\right)_{ref}}\right]^{c_1}\left[\frac{R_t}{\left(R_t\right)_{ref}}\right]^{c_2}\left[\frac{t_b}{\left(t_b\right)_{ref}}\right]^{c_3} \\ char &= \left(char\right)_{ref}\left[\frac{\left(p_c\right)_{ref}}{p_c}\right]^{c_4}\left[\frac{\left(R_t\right)_{ref}}{R_t}\right]^{c_5}\left[\frac{t_b}{\left(t_b\right)_{ref}}\right]^{c_6} \end{aligned} \tag{13}$$

This insulation thickness w_{Th} will usually be enough with phenol type materials to protect the metal structure along the nozzle assembly. The reference values are taken from a sub-scale motor using identical materials and propellant. The coefficients can be calculated from a heat-transfer analysis program or empirically. In order to simplify the calculation of the insulation thickness along the nozzle, a numerical model of the nozzle insulation thickness was built on the basis of a least-squares regression analysis of the results from the heat-transfer computer program. Using this model, the insulation thicknesses along the nozzle can be calculated as a function of the throat thickness w_{Th} only (assuming that c_1-c_6 in Eq. 13 are constant along the nozzle), and therefore a geometric volume model, depending on the one thickness (w_{Th}) can be constructed. Equation 14 describes the nozzle insulation volume as a function of the nozzle parameters (throat radius R_t, exit angle θ_e and expansion ratio ε) and the throat insulation thickness, which is a function of the design parameters (motor pressure and burn time, see Eq. 13). This geometric model simplifies the quick design necessary for the optimization and provides insight to the effect of the various parameters on the insulation mass, where ρ_{ins} is the density of the nozzle insulation. Different nozzles and materials will have different constants. A more accurate (but more complicated) model can be achieved with a series of polynomials for each of the four variables in Eq. 14.

$$V_{ins,noz} = \frac{35 \cdot 10^3}{\rho_{ins}} \left(w_{Th}^{1.0293}\right) \cdot \left(\varepsilon^{0.9262}\right) \cdot \left(\theta_e^{-0.5772}\right) \cdot \left(R_t^{1.9707}\right) \tag{14}$$

Casing mass model:

An expression for the composite casing mass was developed. The mass includes the fore and aft domes and the cylindrical section (Eq. 15):

$$m_{comp} = \frac{p_{max} R^3}{(\sigma/\rho)_{comp}} \left(3\pi \frac{L}{D}\left[3 - \frac{r_{0f}}{r_{0r}}\right] + \frac{(V_{dome})_f}{R^3}\left[3 + \left(\frac{r_{0f}}{R}\right)^2\right] + \frac{(V_{dome})_r}{R^3}\left[3 + \left(\frac{r_{0r}}{R}\right)^2\right] \right) \tag{15}$$

The influence of the opening to casing radius ratio (r_0/R) on the mass of the domes[9] is clearly seen in Eq. 15. The influence of the casing openings ratio (r_{0f}/r_{0r}) on the winding mass of the cylindrical section is based on a netting analysis[11] that calculates the winding width. The consequence of changing the winding angles along the cylinder as a result of a different opening radius ratio influences the hoop and helical winding widths. In any case, the minimum filament mass is obtained when L/D is as small as possible and the casing openings are equal and as small as possible. The penalty will be higher weights of the flanges and forward dome and increased drag losses due to the larger casing diameter.

Casing insulation mass model:

The casing insulation mass is assumed[12] to be a function of the motor pressure and exposed area where the various coefficients are taken from a reference subscale motor having the identical insulation and propellant. The exposed area is obviously affected by the grain design which in turn depends on L/D and the pressure profile (k_p) – hence the $f(L/D, k_p)$ in Eq. 16. The values assumed for the coefficients are: c_7=0.08, c_8=0.5, c_9=0.9. In this work $f(L/D, k_p)$ was assumed to be 1.

$$m_{ins} = c_7 V_{casing}\, p_c^{c_8} t_b^{c_9} f\left(\frac{L}{D}, k_p\right) \tag{16}$$

Other structural elements:

The modeling of the various other structural elements (flanges, forward cover, flexible joint, etc.) can be complicated, but their impact on the design efficiency does not warrant a detailed description. The general approach used for these subsystems is to define the relevant range of variables and materials, and solve the particular subsystem using finite-element design techniques for several points in the range. The appropriate polynomial or power approximation is built on these results.

Flange mass:

$$m_{flange} = 1.15 \rho_{flange} r_0^3 \left(\frac{p_{max}}{\sigma_{flange}}\right)^{0.775} \tag{17}$$

Forward cover mass:

$$m_{str\_fwd\_cover} = 13.3 \rho_{str\_fwd\_cover} r_{0f}^3 \left(\frac{p_{max}}{\sigma_{str}}\right) \tag{18}$$

Flexible joint mass model:

$$m_{joint} = 23.25\left(R_t + w_{Th}\right)^3 p_{max} \tag{19}$$

Nozzle metal assembly:

$$m_{noz\_str} = 21.18\,\rho_{noz\_str} R_t^{\,2}\left(\frac{p_{max}}{\sigma_{noz\_str}}\right)^{0.861} \tag{20}$$

Other inert masses:

Other inert masses (igniter, actuators, external insulation, skirts, etc.) were assumed be 2% of the propellant mass.

Maximum web constraint:

The sources of the strain in the propellant grain are the slow cool-down (after polymerization), the changing storage conditions and the motor pressure during operation. It is desirable to have a high a web fraction (WF) as possible, which is limited by the maximum strain. Using a strain analysis program, a matrix of different cylindrical grains of finite length were analyzed. The parameters that were varied in these runs included L/D, maximum ignition pressure, cool-down[13]. The maximum strain was set at 30%, and a 2nd degree polynomial for the maximum web fraction was created (Eq. 21) from the results.

$$WF_{max} = 1 - \left[\Phi_1\left(\frac{L}{D}\right)^2 + \Phi_2\left(\frac{L}{D}\right) + \Phi_3\right] \tag{21}$$

The coefficients Φ_i are a function of the maximum pressure:

$$\begin{cases} \Phi_1 = 1.684\cdot 10^{-6}\, p_{max}^2 - 1.205\cdot 10^{-5}\, p_{max} + 5.200\cdot 10^{-5} \\ \Phi_2 = -3.729\cdot 10^{-4}\, p_{max}^2 + 2.354\cdot 10^{-3}\, p_{max} - 5.859\cdot 10^{-3} \\ \Phi_3 = 8.088\cdot 10^{-3}\, p_{max}^2 - 2.569\cdot 10^{-2}\, p_{max} + 2.086\cdot 10^{-1} \end{cases}$$

To ensure that no erosive burning exists, the port radius must be at least 40% greater than the throat radius:

$$1 - 1.4\frac{R_t}{R} < WF \tag{22}$$

Maximum casing openings:

The maximum ratio of the casing openings is limited by the slip coefficient of the filament on the cylinder[9], and can be presented as a 2nd degree polynomial (Eq. 23):

$$\frac{1}{r_{0f}} - \frac{1}{r_{0r}} \le \frac{C_f L}{R^2} \Rightarrow \left(\frac{r_{0f}}{r_{0r}}\right)_{max} = 1 - 0.77\left(2\frac{L}{D}\frac{r_{0r}}{R}c_f\right) + 0.26\left(2\frac{L}{D}\frac{r_{0r}}{R}c_f\right)^2 \tag{23}$$

Propellant burn rate limits:

The burn rate of the propellant in a motor is calculated by dividing the propellant web by the burn time ($R\cdot WF/t_b$). It is assumed that the minimum and maximum burn rates at 70 atm are 5 and 20 mm/sec, respectively.

This page has been purposedly left blank